Investigation of nano-microstructural changes in Maastricht limestone after treatment with nanolime suspension

Radek Ševčík[1], Alberto Viani[1], Lucia Mancini[2], Marie-Sousai Appavou[3], Dita Machová[1]

[1] Institute of Theoretical and Applied Mechanics of the Czech Academy of Sciences, Prosecká 809/76, 190 00 Praha, Czech Republic

[2] Elettra-Sincrotrone Trieste S.C.p.A., S.S. 14-km 163.5 Area Science Park, Trieste, Basovizza, Italy

[3] Forschungszentrum Jülich GmbH, Jülich Centre for Neutron Science JCNS, Aussenstelle am MLZ, Lichtenbergstraße 1, Garching, Germany

Corresponding author: R. Ševčík; sevcik@itam.cas.cz

Abstract

Nanolimes are dispersions of nanosized $Ca(OH)_2$ particles in alcohols often used for the consolidation of various types of cultural heritage objects. The consolidation effect is based on the transformation of $Ca(OH)_2$ into $CaCO_3$ phases during carbonation process. The detection of microstructural changes consequent to a consolidating treatment (essential to evaluate its effectiveness), was approached adopting the innovative combination of two advanced techniques, covering a range in pore size from the nanometric to the millimetric scale: small angle neutron scattering (SANS) and synchrotron X-ray micro-computed tomography (μ-CT). The changes in the 3D microstructure of samples of Maastricht limestone, a well-known weak stone material considered as a sort of 'standard' in cultural heritage conservation studies, pure and treated with nanolime dispersions, have been described in a fully non-invasive fashion, overcoming the limitation of previous approaches. The application of nanolime resulted to have a limited positive effect in reducing the fine porosity. Its time-evolution was attributed to the progress of the carbonation reaction. On the contrary, the treatment produced positive effects on the porosity in the size range covered with μ-CT, reducing the pore accessibility between 30 and 65 μm, suggesting an

improvement of the mechanical properties. The combined use of SANS and μ-CT represents and novel methodological approach in support of cultural heritage conservation works.

Keywords: Limestone; nanolime; consolidation; porosity; neutron scattering; X-ray tomography.

1 Introduction

Lime-based materials, which harden thanks to the conversion of $Ca(OH)_2$ into calcium carbonate ($CaCO_3$), which occurs by intervention of atmospheric CO_2, have encountered the favour of practitioners as consolidating agents to be employed in the preservation of cultural heritage objects. They are preferred to organic polymers and alkoxysilanes, used in the past, because of their better compatibility with many substrates, an aspect which is now recognized decisive in the conservation practice [1-4]. Between the lime-based products on the market, the performance of the recently proposed alcoholic suspensions of nanosized $Ca(OH)_2$ stands out when compared to traditional applications of lime water [2-4]. They possess much higher surface area and reactivity, and don't show the downsides of the latter, such as the high volume of water and high number of application required [1]. For this reason, their range of application spans from preservation of stones and wall paintings, to wooden objects, manuscripts and canvas [3].

The carbonation of $Ca(OH)_2$, is a multistep process (described e.g. in [5]), whose rate strongly depends on the conditions of temperature, relative humidity, degree of supersaturation, ion concentration, ionic strength, type and concentration of additives/impurities and may result in different $CaCO_3$ polymorphs [6-8]. From them, three anhydrous crystalline phases are known: calcite, aragonite and vaterite [8-9].

One major problem encountered in the conservation practice is the evaluation of the effectiveness of the treatment, especially when considering that almost every application substrate has unique characteristics and that this type of investigation should be ideally accomplished without perturbing the sample. Electron and/or optical microscopy are by far the most frequented approaches to the task. Unfortunately, they suffer from lack of representativeness, because of the small volume investigated, the objective difficulty in recognizing the newly formed carbonates in matrices containing already calcium carbonate (e.g. carbonatic rocks), lack of quantitative description of an adequate volume of sample and a relatively invasive sample preparation. Widely used mercury intrusion porosimetry may cause the modification of the inner matrix of fragile samples, due to penetration of liquid mercury under high pressures into the pore matrix. Other invasive approaches, like e.g. measurements of drilling resistance, or compressive strength are not suitable for valuable samples originating from cultural heritage objects, when only very limited amount of material can be collected. The overview of other techniques used for the evaluation of consolidation procedure are described in [1] and references therein.

In this paper, the innovative combination of small angle neutron scattering (SANS) and synchrotron radiation X-ray micro-computed tomography (μ-CT) is employed to quantitatively describe, in a fully non-invasive fashion, microstructural changes induced in a porous rock by a consolidation treatment with nanolime.

2 Experimental

The Maastricht limestone is a calcarenite stone employed in construction in northern Europe (mostly in Belgium and The Netherlands) well-known for its high porosity [10]. Untreated fresh Maastricht limestone was used as reference material. In order to limit multiple scattering effects during SANS measurement, and cover a representative volume in reasonable time

during µ-CT data collection, two different shapes of samples were used for the experiments, as depicted in Fig. 1.

Consolidation treatment was done by two applications of 391 µl (or 118 of µl in case of smaller µ-CT specimens) commercial nanolime suspension (CaLoSil E25, $c_{Ca(OH)2}$ = 25 g l^{-1}, IBZ – Salzchemie). The second treatment was done after 24 hours. Prepared samples (see Fig. 1) were kept in climate chamber under controlled conditions of 65(5) % RH, 20(1) °C and 450(50) ppm CO_2 for 6 weeks. In case of SANS measurements, also the changes in nano/microporosity during the development of carbonation reaction were studied, investigating samples aged for 3 days, 3 and 6 weeks.

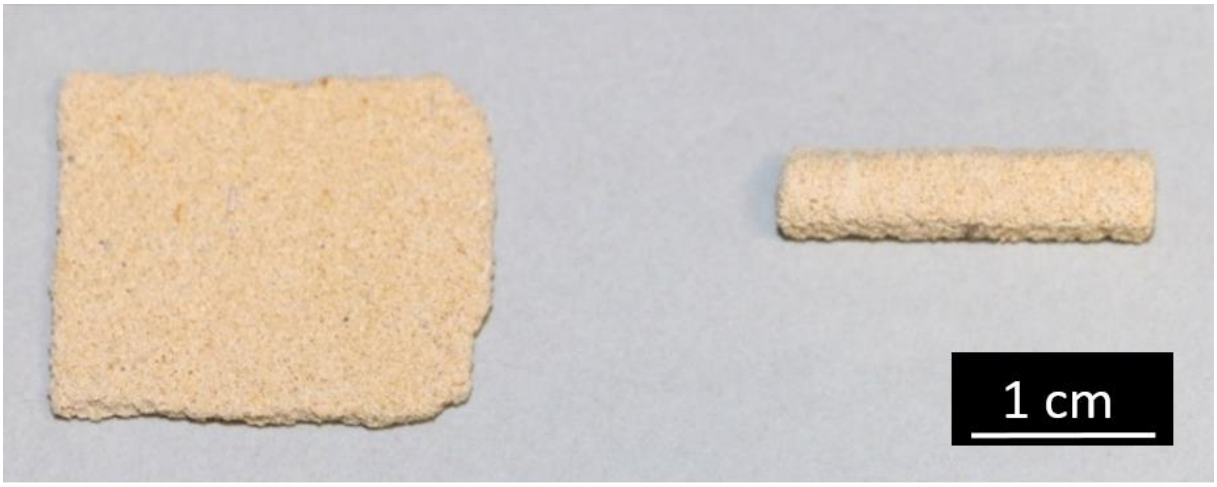

Fig. 1. The visualization of samples of Maastricht limestone used for SANS (on the right) and µ-CT testing (on the left).

The slices prepared from fresh Maastricht limestone for investigation with SANS technique were about 2 mm thick to reduce the effect of multiple scattering. Data were collected at two different wavelengths (λ = 5.0 and λ = 10.0 Å) as dependence of intensity (I) on the scattering angle 2θ in the Q range 0.0015−0.4500 $Å^{-1}$.

Q is defined as:

$$Q = \frac{4\pi}{\lambda} \sin 2\theta \qquad (1)$$

Data were acquired using three sample-to-detector distances (1.5, 8 and 20 m) with the KWS-2 instrument [11] at JCNS at the Heinz Maier-Leibnitz Zentrum MLZ in Garching (Germany). Raw data were converted to absolute scale using signals from empty beam and black matter and, finally, data collected at different distances were merged together using QtiKWS software developed by JCNS. The 1-D scattering curves (I vs. momentum transfer (Q)) are obtained by radial averaging of the data in the 2-D patterns collected at the detector. From 1-D SANS curves, information about the shape and size distribution of the scatterers (in our case, pores) can be retrieved. For the description of the complex microstructure of porous solids, a spherical form factor for the pores, is usually adopted [12-14]. Under this assumption, the volume weighted pore size distribution can be obtained through the fit of the SANS curves [15-17]. To this aim, the software McSAS [18], implementing a procedure based on the Monte Carlo method, has been employed.

In a SANS experiment, the detected intensity depends on the scattering contrast (function of the strength of the interaction of the neutrons with matter) in the investigated volume of sample. The latter is defined by the beam spot size (around 1 cm) and thickness. The technique is fully non-invasive, representing an attractive alternative to other methods for detecting porosity in solid matrices. In most cases, a representative volume of sample can be probed. A detailed theoretical background on the technique is outside the scope of the present article, and can be found elsewhere [19]. It is here worth noting that, in a porous solid, the scattering contrast arises because of the difference in scattering strength between the matrix and the air in pores (being the latter negligible). The size of the scattering objects (pores) is inversely proportional to Q, and, at high Q ($Q \gg {}^{1}/_{R}$, where R is the object radius), irrespectively of the pore shape, the SANS curve depends solely on the surface characteristics of the pores. In a double logarithmic plot $I(Q)$ vs. Q, a change in slope of the curve marks the boundary between two different surfaces corresponding to different length scales. The

analysis of the slopes is therefore conveying information about the multiscale nature of the microstructure [20]. Within one scattering regime, the SANS curve can be described by a power law:

$$\lim_{Q\to\infty} I(Q) = B\left(\frac{1}{Q}\right)^{n} \quad (2)$$

The exponent n in Eq. 2 is a measure of the fractal nature of the scattering objects [21]. When $1 < n < 3$, we have mass (or volume) fractals with fractal dimension $D = n$. When $3 < n < 4$, we have surface fractals, with fractal dimension $D_S = 6 - n$. The exponent $n = 4$ for sharp and smooth surfaces. In this case, the scattered intensity becomes proportional to the specific surface per unit volume of sample [22].

μ-CT data were obtained at the SYRMEP beamline located at the Elettra Sincrotrone facility (Trieste, Italy). Overall, 3000 X-ray tomographic projections have been collected for each sample in region-of-interest mode over a full rotation of 360°. Two replicates and 2 vertically displaced volumes for each sample were measured with an effective pixel size of 1.4 μm × 1.4 μm in phase-contrast mode and sample-to-detector distance of 150 mm [23-24] with 1 s exposure/projection time. The images reconstruction, processing and quantitative image analysis were conducted with software packages developed at Elettra [25-27]. More detailed description of the data treatment can be found elsewhere [14,28]. An anisotropic diffusion filter followed by image segmentation with the automatic Otsu's method [29] have been adopted to allow for the pore identification. In order to reduce the computation time during quantitative image analysis, a suitable volume of interest was determined by calculating Representative Elementary Volumes for each sample. The calculated sample parameters obtained were: porosity (Φ) [%], specific surface area (S_V [mm^{-1}]) and fractal dimension (D). The latter, is reflecting the fractal nature of the pores, according to the fractal theory [21], in the same way as for the analysis of the slope of the SANS curves described above. Moreover, the MIP simulations and the unconstrained pore size distribution (PSD)

obtained from 3D continuous approach, as detailed in [30], were calculated using the Pore Size Distribution plugin [31] implemented in Fiji software [32]. The pore accessibility of samples was determined by the ratio between PSD obtained from MIP simulations and PSD calculated using 3D continuous approach [30]. Therefore, its value is sensitive to the presence of 'necks' in the connected open pore network, which impair fluid penetration.

X-ray powder diffraction using D8 Advance diffractometer (Bruker AXS) in Bragg-Brentano geometry was employed to define the mineralogical composition of the untreated stone. Voltage and current of X-ray generator were set to 40 kV and 40 mA, respectively. Data were collected on a LynxEye 1-D silicon strip detector. CuK_{α} radiation was selected through a Ni filter. Samples were measured at laboratory temperature in the angular range 15-90º 2θ with a virtual step scan of 0.01º, counting 0.4 s per step and spinning the sample at 15 rpm (in order to obtain better particle statistics). Rietveld refinement method [33] implemented in software Topas 4.2 (Bruker AXS) was employed in order to perform quantitative analysis of mineral phases (QPA).

3 Results and discussion

The QPA using Rietveld refinement on fresh Maastricht limestone revealed that the average composition was 99.8 wt. % of calcite and 0.2 wt. % of quartz. Thus, the consolidation with $Ca(OH)_2$ nanoparticles fully meets the requirement of compatibility with substrate, because, after some time, they transform into $CaCO_3$, as mentioned above. The detailed characterization of the used nanolime suspension, CaLoSil E25, is described e.g. in [8].

SANS measurements revealed very small changes in the obtained data. As an example, in Fig. 2, the SANS curve pertaining to the sample of Maastricht limestone treated with CaLoSil E25 and carbonated for 3 weeks, is illustrated, together with the best fit obtained with the McSAS software. The analysis of the slope of the scattering curves scales revealed the

presence of two scattering regimes in all the samples: one at low Q, characterized by slope -4 (Porod regime), connected to a partially resolved Guinier regime (the region where the curve flattens), and one at high Q, with slope between -3 and -4 (see Table 1). According to the fractal interpretation, the former indicates a smooth pore surface and the latter a surface fractal. The increase in fractal dimension D_S after the treatment corresponds to an increase in the complexity of the pore surface (in this range of sizes). A slight but detectable decrease of D_S with time, likely reflects the progressive development of calcium carbonate, with a reduction of the pore surface roughness.

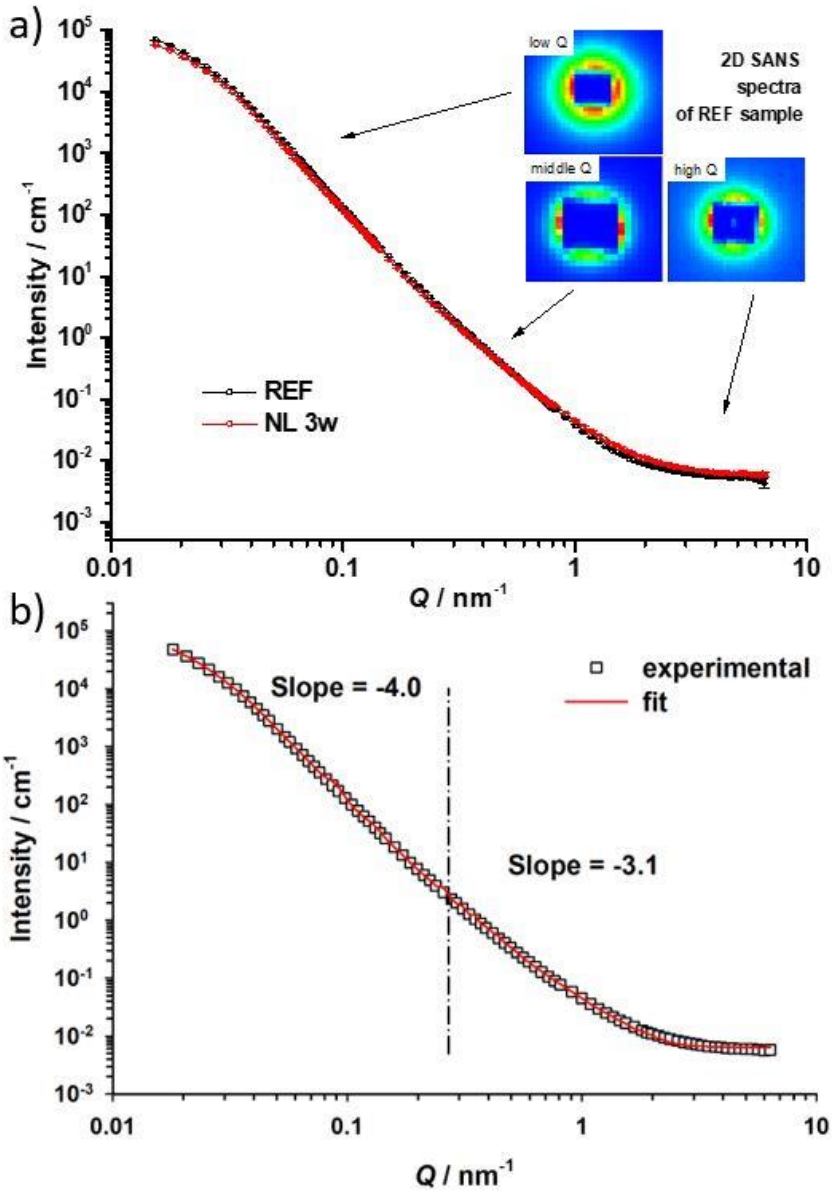

Fig. 2. Normalized 1D SANS curves of (a) the untreated sample of Maastricht limestone and samples treated with nanolime kept in climate chamber for 3 weeks. In the inset of Fig.2a are shown 2D spectra of REF sample collected at three different sample to detector distances. Normalized 1D REF spectrum was produced by merging of three curves obtained from radial averaging of appropriate 2-D patterns and (b) example of one of measured SANS curve of Maastricht limestone samples consolidated with nanolime suspension and carbonated for 3 weeks in climate chamber. As dotted symbols are presented experimentally obtained data (standard errors within symbols) and the best fit is reported as continuous line. The Monte Carlo method implemented in McSAS software was used for the fit. The regions with different regimes are labeled.

To retrieve a quantitative information about the porosity of samples, in the range covered by the experiment, the fit of the SANS data was accomplished calculating the scattering contrast for neutrons, assuming $CaCO_3$ and air (present in pores). Results of the fit with the McSAS software are depicted in Fig. 3. It can be observed that the pores of sound and treated samples were distributed mainly around 200 nm with some negligible amount of pores with radius between 2 and 20 nm.

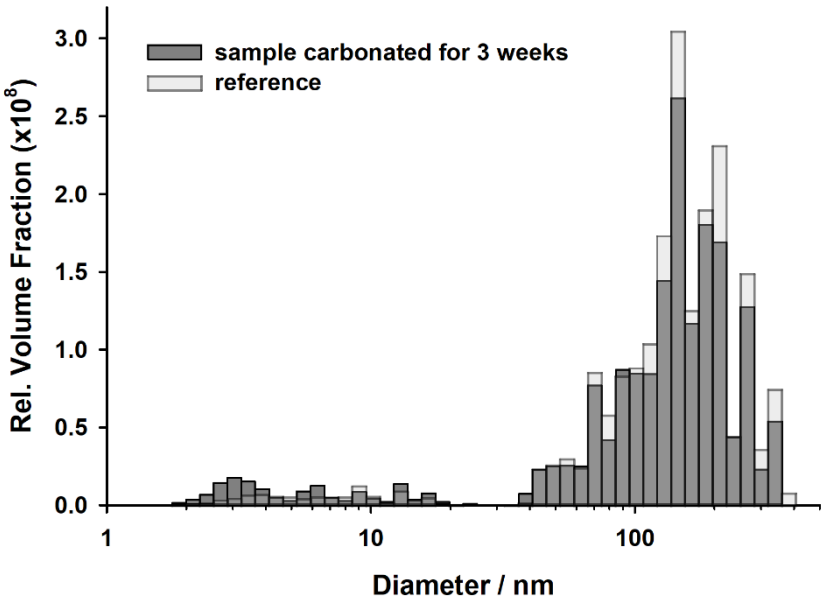

Fig. 3. Volume-weighted pore size distributions as determined from SANS curves of treated samples carbonated for 3 weeks. It can be noted that nanolime treatment slightly decreased the radius of pores in the region around 200 nm.

These findings are in line with the results recently obtained using nanolime additivated with synthetic $CaCO_3$ polymorphs particles [17]. As reported in Table 1, the total porosity was decreasing with increasing carbonation time. However, at variance with this trend is the value relative to the samples collected after 6 weeks of carbonation time, exhibiting porosity comparable with the untreated sample. The reason could be the heterogeneity of the Maastricht limestone microstructure and the presence of many fossils of variable size (see Fig. 4 – images from µ-CT measurements) hosting closed porosity. In fact, SANS is sensitive to both types of pores. It can be argued that the results obtained from the samples after the treatment are not so positive because 'diluted' by the contribution of the closed pores, not accessible to the consolidant. Taking advantage of the SANS contrast variation technique, already applied for different $CaCO_3$ system [34], the contribution of the open porosity can be obtained [35]. After soaking the sample in a mixture of D_2O and H_2O, calculated to exactly match the scattering contrast of the solid matrix ($CaCO_3$), the neutrons shall 'see' only the closed pores, therefore, by subtracting this signal to the one from the dry sample (hosting open and closed pores), the open porosity can be retrieved. It must be concluded that to correctly describe the evolution of nanoporosity during the carbonation reaction of nanolime, new experiments (which are already planned) and on more replicates, will be needed.

The µ-CT measurements were performed on untreated samples and samples treated with CaLoSil E25 cured for 6 weeks in climate chamber. An example of the axial view after reconstruction of the VOI of REF sample is depicted in Fig. 4a. Cross-sectional axial 2D section µ-CT segmented images collected for untreated sample before and after filtering, are shown in Fig. 4b and Fig. 4c, respectively. The pore network is characterized by a high number of pores, with size up to 400 µm, and showing high connectivity. It can be noticed that the high amount of fossils adds a fraction of pores, mostly closed, as mentioned above. In case of one REF replicate, a massive dense solid was revealed within the inner structure of

Maastricht limestone (Fig. 4c). This volume, as well as those with very large fossils, were excluded in the choice of the VOI for all the samples. The calculated values of porosity (Table 1) indicated a slight decrease after the application of nanolime. The values of surface per unit volume (S_V) were found to be the same (Table 1). The total porosity, as in case of SANS including open and closed pores, decreased from 47.1 % found in fresh Maastricht limestone to 46.6 % for treated one. Therefore, in the range of pore sizes accessible to the experiment, despite the low amount of nanolime applied to the sample, a detectable decrease in porosity was observed. It is well documented that improvement of mechanical properties of the treated materials can be obtained by slight reduction of porosity [36-37]. This result is even more significant when considering that the volume investigated did not include the sample surface, always affected by accumulation of particles with limited effect on bulk properties.

When considering the fractal dimension, it was found to increase from 2.721 to 2.731 after the treatment. Since the difference exceeds the experimental error, this should reflect the effect of the treatment, similarly to what observed for the SANS data, and corresponds to an increase in surface roughness and/or in its complexity. Notably, a difference in fractal dimension exists between SANS and µ-CT. This is due to the different length scales probed by the two techniques and reflects the multiscale nature of the pore network, as commonly observed in rocks [38].

Therefore, it must be assumed that for length scales exceeding 200−220 nm (Fig. 3), the nature of the pore surface changes from smooth (low-Q regime with n=4 in Fig. 2), to surface fractal (D_S= 2.721). A change in scattering regime is testified by the Guinier 'knee' exhibited by the SANS curves at very low Q. However, it should not be forgotten that a gap in pore size exists between current SANS and µ-CT data.

The pore accessibility test is an alternative way to quantitatively evaluate the effect of the treatment. This test is a measure of the changes in the number and size of pores which are

accessible from outside the selected volume, relying on the data from the 3D microstructure obtained from the VOIs (Fig. 4c). The main advantage, in the present case, is that the closed porosity is excluded in the calculation. As observed in Fig. 5c, a decrease in pores accessibility for pores with size between 30 to 65 µm, after the treatment, is clearly visible.

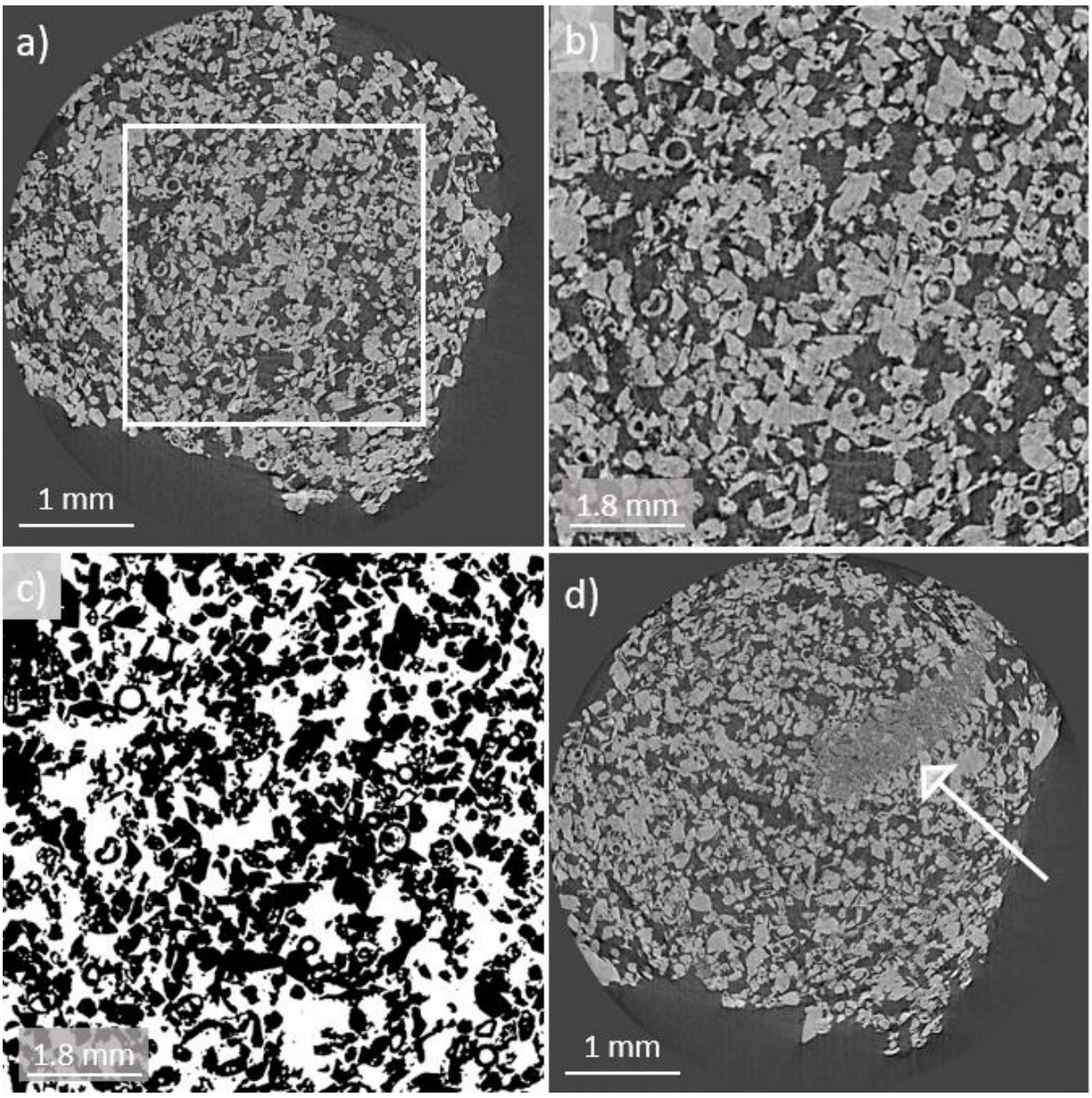

Fig. 4. Selected axial view of untreated Maastricht limestone sample (reference) with clearly visible large pores and fossils (a) and highlighted volume of interest with white rectangular. The same image after segmentation before (b) and after filtering (c) used for the quantitative image analysis. In one replicate of REF, the dense solid heterogeneity was detected (highlighted by arrow) in the volume of sound limestone in (d)).

Table 1. Porosity (Φ), slope at high Q and fractal dimension (D_S) from SANS data and porosity, surface per unit volume (S_V) and fractal dimension (D) from µ-CT data. (REF = untreated Maastricht limestone samples, NL = samples treated with nanolime, 3d = 3 days of carbonation, 3w = 3 weeks of carbonation, 6w = 6 weeks of carbonation).

Sample	SANS			µ-CT		
	Φ [a] / %	Slope (α, at high Q)	D_S [c]	S_V / m^{-1}	Φ [a] / %	D
REF	0.198 ± 0.001	-3.37	2.63	41 ± 1	47.1 ± 0.01 [b]	2.721 ± 0.005
NL 3d	0.188 ± 0.001	-3.09	2.91	-	-	-
NL 3w	0.175 ± 0.001	-3.13	2.87	-	-	-
NL 6w	0.199 ± 0.001 [b]	-3.22	2.78	41 ± 1 b	46.6 ± 0.01 [b]	2.731 ± 0.002

[a] Percentage of the volume of pores to the total sample volume. [b] Average values from two replicates. [c] SANS fractal dimension (D_S) calculated from slope (high Q) as described in the experimental part.

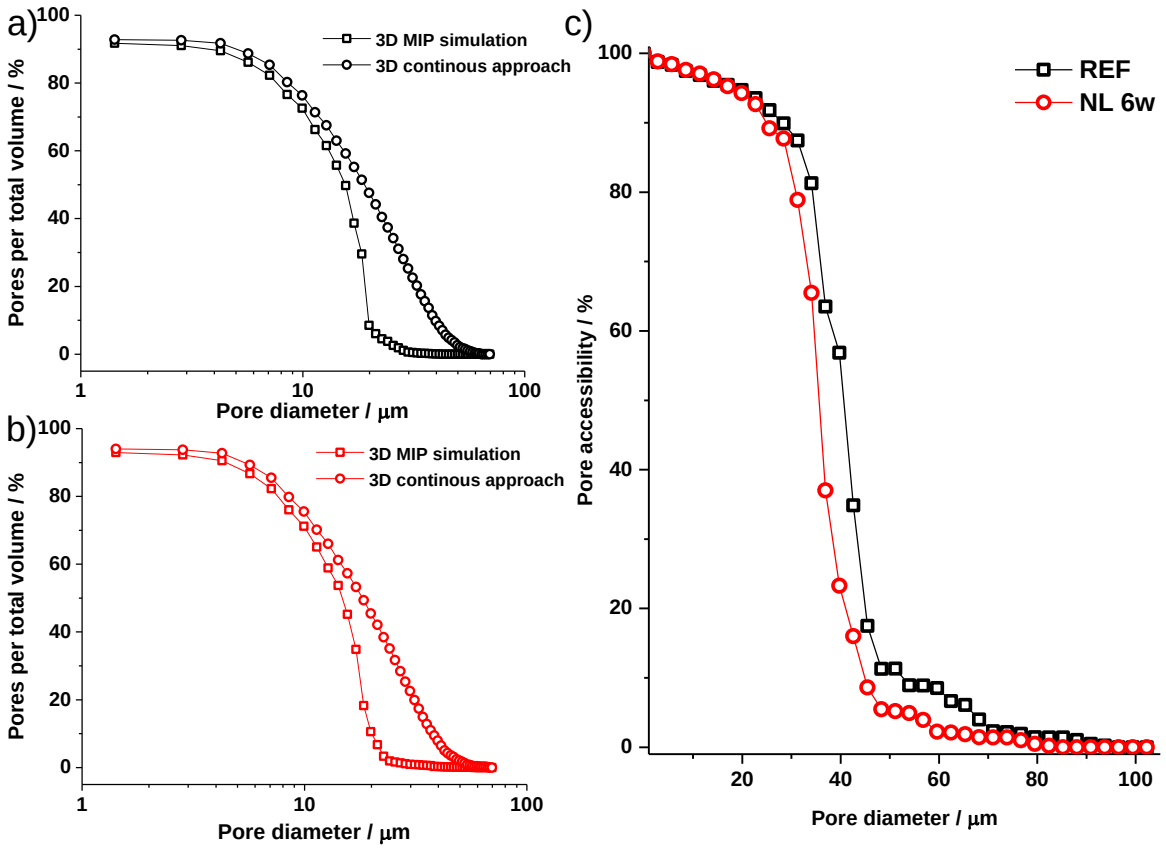

Fig. 5. Comparison of the cumulative distribution function of intra-aggregate porosity based on the 3D MIP simulation and 3D continuous approach of reference sample (REF) (a) and sample treated with nanolime and carbonated for 6 weeks (NL 6w) (b). Pore accessibility ratios for REF and NL 6w samples calculated for the intra/aggregate pore space (c). Spherical entities were used for the mathematical simulations.

All in all, the combination of both techniques, SANS and X-ray µ-CT, can be considered appropriate for the characterization of nano/microstructural changes after the consolidation procedures. When the specific case is considered, the results, especially from the SANS technique, indicated that the effect of the consolidation treatment was not very significant, due to the coarse sample microstructure, hosting a very small nanoporosity and with heterogeneities at the scale of mm. Nonetheless, the pore accessibility test clearly indicated that, when the contribution of closed pores is factored out, the effect of the treatment with

nanolime can be detected as reduced accessibility, which should imply changes in dynamical properties, such as water absorption. It must be noted that the employed stone shows most of the porosity in a range of sizes rather big for the nanomaterial employed, so, also the impact of the treatment on the total porosity was necessarily very small. As already pointed out, the consolidation treatments of very porous stones with nanolime have to be performed with sufficient volumes of consolidant and, usually, several cycles of application are needed to strengthen the material [1]. In the present case, a relatively small amount of consolidating agent has been employed, in order to test the sensitivity of the techniques and reduce unwanted effects caused by multiple treatments. In fact, the consolidation of very porous stones with nanoparticles brings some drawbacks. Most importantly, partial back migration of particles and their accumulation on the surface of treated materials, causing formation of white haze [1,39]. A solution to eliminate this back migration effect has not been found yet [39-40] since none of the proposed solutions appears as conclusive. More recently, different approaches to suppress this negative effect were tested. The treatment with nanolime additivated with different $CaCO_3$ polymorphs, namely calcite, vaterite and aragonite, resulted in higher decrease in porosity, respect to application of nanolime alone [17]. In addition, SEM observations revealed good compatibility within the chemically similar system composed of nanolime, $CaCO_3$ particles and limestone. Larger $CaCO_3$ particles helped nanolime particles in bridging the limestone grains. The type of $CaCO_3$ polymorphs introduced, also controlled the type of newly formed $CaCO_3$ polymorphs [41]. This is of relevance in consideration of their different physical-mechanical properties [42]. Recently, nanolime suspensions have been additivated with nanocalcite in presence of polymeric dispersant [43] or with larger $Ca(OH)_2$ particles [44]. As already reported, the nanolime treatment may be more effective when the proper choice of type or mixture of solutions, is made [29, 45-47]. In highly porous matrix, it was shown that reciprocal mixture of isopropanol and water resulted in slightly better

reduction of porosity and increasing in strength in comparison with other tested solvents [47]. As a final remark, it may be noted that the treatment with nanolime should be always tuned according to the treated substrate to assure the possible best conservation action that will prevent the valuable object of cultural heritage to our future generations.

4 Conclusion

The combination of the SANS and phase-contrast synchrotron X-ray μ-CT techniques was, for the first time, used for the quantitative characterization of nano/microstructural changes of Maastricht limestone`s samples after the consolidation treatment with nanolime suspension. The SANS technique showed that the samples were consisting of two structures in the range of sizes covered: smooth pore surface and a surface fractal. After the treatment, the complexity of the pore surface increased and evolved in time. A small, but detectable, decrease of the porosity during nanolime carbonation in the Maastricht limestone, was observed. However, for the definitive confirmation more replicates have to be measured due to the heterogeneity of the natural stone. The μ-CT measurements clearly showed a decrease in porosity, even if the amount of nanolime employed was very small.

This experimental approach has the advantage of being fully non-invasive offering the possibility of detecting nano/microstructural changes in very small specimens. The combination of these two techniques was found to effectively cover a wide range in porosity and it could be used also for samples obtained from cultural heritage objects needing or undergoing conservative treatments. The future research shall include the use of ultra-SANS, which allows to extend the observed range of porosity towards higher sizes (up to 2-4 μm) to fully cover the pore size-gap between the two techniques employed, and the adoption of contrast variation, as mentioned in the previous section.

Acknowledgement

The authors thank the Czech Science Foundation GA ČR (grant number 17-05030S) for financial support, the Heinz Maier-Leibnitz Zentrum (MLZ in Garching, Germany) for the beamtime provided at the KWS-2 instrument operated by JCNS in the frame of a regular proposal and CERIC-ERIC Consortium for the access and travel support to the Elettra Sincrotrone facility (Trieste, Italy).

References

1. R. van Hees, R. Veiga, and Z. Slížková, Mater. Struct. Constr. 50, 1 (2017).

2. C. Rodriguez-Navarro and E. Ruiz-Agudo, Pure Appl. Chem 90, 523 (2018).

3. P. Baglioni, D. Chelazzi, and R. Giorgi, Nanotechnologies in the Conservation of Cultural Heritage (Springer Netherlands, Dordrecht, 2015).

4. G. Ziegenbalg, M. Drdácký, C. Dietze, and D. Schuch, Nanomaterials in Architecture and Art Conservation, 1st ed. (Pan Stanford Publishing, Singapore, 2018).

5. Ö. Cizer, C. Rodriguez-Navarro, E. Ruiz-Agudo, J. Elsen, D. Van Gemert, and K. Van Balen, J. Mater. Sci. 47, 6151 (2012).

6. P. López-Arce, L. S. Gómez-Villalba, S. Martínez-Ramírez, M. Álvarez de Buergo, and R. Fort, Powder Technol. 205, 263 (2011).

7. S. M. Shih, C. S. Ho, Y. S. Song, and J. P. Lin, Ind. Eng. Chem. Res. 38, 1316 (1999).

8. C. Rodriguez-Navarro, K. Elert, and R. Ševčík, CrystEngComm 18, 6594 (2016).

9. F. Lippmann, in Sediment. Carbonate Miner. Miner. Rocks Inorg. Mater. (Monograph Ser. Theor. Exp. Stud. (Springer, Berlin, Heidelberg, 1973), pp. 5–96.

10. C. D. Wim, D. Michiel, D. Dreesen, F. M. Werner, and N. G. Timo, in Int. Conf. Heritage, Weather. Conserv. (2006), p. 9.

11. A. Radulescu, N. K. Szekely, and M.-S. Appavou, J. Large-Scale Res. Facil. JLSRF 1, 29 (2015).

12. A. J. Allen, J. Am. Ceram. Soc. 88, 1367 (2005).

13. A. Viani, R. Ševčík, M. S. Appavou, and A. Radulescu, Appl. Clay Sci. 166, 1 (2018).

14. A. Viani, K. Sotiriadis, A. Len, P. Šašek, and R. Ševčík, Mater. Charact. 116, 33 (2016).

15. A. Viani, K. Sotiriadis, P. Šašek, and M. S. Appavou, Ceram. Int. 42, 16310 (2016).

16. A. J. Allen, S. Krueger, G. G. Long, H. M. Kerch, H. Hahn, and G. Skandan, Nanostructured Mater. 7, 113 (1996).

17. R. Ševčík, A. Viani, D. Machová, G. Lanzafame, L. Mancini, and M. S. Appavou, Sci. Rep. 9, 1 (2019).

18. I. Bressler, B. R. Pauw, and A. F. Thünemann, J. Appl. Crystallogr. 48, 962 (2015).

19. P. Staron, A. Schreyer, H. Clemens, and S. Mayer, editors , Neutrons and Synchrotron Radiation in Engineering and Material Science (Wiley-VCH Verlag GmbH, Weinheim, 2017).

20. P. W. Schmidt, J. Appl. Crystallogr. 24, 414 (1991).

21. B. B. Mandelbrot, The Fractal Geometry of Nature (W.H. Freeman, San Francisco, 1982).

22. G. Porod, in Small Angle X-Ray Scatt., edited by O. Glatter and O. Kratky (Academic Press Inc., London, 1982), pp. 17–51.

23. S. W. Wilkins, T. E. Gureyev, D. Gao, A. Pogany, and A. W. Stevenson, Nature 384, 335 (1996).

24. P. Cloetensdag, B. Raymondm, B. José, G. Jean-Peirre, and S. Michel, J. Phys. D. Appl. Phys. 29, 133 (1996).

25. F. Brun, S. Pacilè, A. Accardo, G. Kourousias, D. Dreossi, L. Mancini, G. Tromba, and R. Pugliese, Fundam. Informaticae 141, 233 (2015).

26. F. Brun, L. Massimi, M. Fratini, D. Dreossi, F. Billé, A. Accardo, R. Pugliese, and A. Cedola, Adv. Struct. Chem. Imaging 3, 4 (2017).

27. F. Brun, L. Mancini, P. Kasae, S. Favretto, D. Dreossi, and G. Tromba, Nucl. Instruments Methods Phys. Res. Sect. A Accel. Spectrometers, Detect. Assoc. Equip. 615, 326 (2010).

28. A. Viani, K. Sotiriadis, I. Kumpová, L. Mancini, and M. S. Appavou, Dent. Mater. 33, 402 (2017).

29. N. Otsu, IEEE Trans. Syst. Man. Cybern. 9, 62 (1979).

30. P. Trtik, M. Soos, B. Münch, A. Lamprou, R. Mokso, and M. Stampanoni, Langmuir 27, 12788 (2011).

31. B. Münch and L. Holzer, J. Am. Ceram. Soc. 91, 4059 (2008).

32. J. Schindelin, I. Arganda-Carreras, E. Frise, V. Kaynig, M. Longair, T. Pietzsch, S. Preibisch, C. Rueden, S. Saalfeld, B. Schmid, J. Y. Tinevez, D. J. White, V. Hartenstein, K. Eliceiri, P. Tomancak, and A. Cardona, Nat. Methods 9, 676 (2012).

33. H. M. Rietveld, J. Appl. Crystallogr. 2, 65 (1969).

34. V. Pipich, M. Balz, S. E. Wolf, W. Tremel, and D. Schwann, J. Am. Chem. Soc. 130, 6879 (2008).

35. H. Brumberger, editor, Modern Aspects of Small-Angle Scattering, 1st ed. (Springer Science & Business Media., 1995).

36. R. A. Al-Omary, M. Al-Naddaf, and W. Al Sekhaneh, Mediterr. Archaeol. Archaeom. 18, 35 (2018).

37. J. Jang and F. G. Matero, J. Am. Inst. Conserv. 57, 95 (2018).

38. L. M. Anovitz and D. R. Cole, Rev. Mineral. Geochemistry 80, 61 (2015).

39. G. Borsoi, B. Lubelli, R. van Hees, R. Veiga, and A. Santos Silva, Constr. Build. Mater. 142, 385 (2017).

40. K. Niedoba, Z. Slížková, D. Frankeová, C. Lara Nunes, and I. Jandejsek, Constr. Build. Mater. 133, 51 (2017).

41. R. Ševčík, P. Mácová, M. P. Estébanez, and A. Viani, Constr. Build. Mater. 228, 116802 (2019).

42. R. Ševčík, P. Šašek, and A. Viani, J. Mater. Sci. 53, 4022 (2018).

43. M.-B. Coltelli, D. Paolucci, V. Castelvetro, S. Bianchi, E. Mascha, L. Panariello, C. Pesce, J. Weber, and A. Lazzeri, Nanomaterials 8, 254 (2018).

44. J. Otero, V. Starinieri, and A. E. Charola, Constr. Build. Mater. 209, 701 (2019).

45. G. Borsoi, B. Lubelli, R. van Hees, R. Veiga, and A. S. Silva, Appl. Phys. A Mater. Sci. Process. 122, 1 (2016).

46. G. Borsoi, B. Lubelli, R. van Hees, R. Veiga, A. S. Silva, L. Colla, L. Fedele, and P. Tomasin, Colloids Surfaces A Physicochem. Eng. Asp. 497, 171 (2016).

47. J. Otero, V. Starinieri, A. E. Charola, and G. Taglieri, Constr. Build. Mater. 230, 117112 (2020).